Solar Energy Concentration for Thermoelectric Power Generation at the Sub-Dekawatt Scale

Christie M. Fallwell[1], Dylan W. Davis[2], and Matthew J. Traum[3]
University of North Texas, Denton, TX 76201

High temperature reduces photovoltaic (PV) generator efficiency, but it improves thermoelectric (TE) generator efficiency. This behavior is an important consideration for remote, solid-state, sub-dekawatt solar concentrating generators, which focus enormous power onto small target areas. Resulting temperatures exceed the threshold beyond which TEs become a competitive alternative to PVs. Using simple temperature-dependant analytical PV and TE models, we found that TE efficiency exceeds PV efficiency for temperatures above 495 K, corresponding to collector-to-target area ratios exceeding 4.7. To experimentally validate these models, an apparatus was built using a square Fresnel concentrating lens 28.8 times the area of the target generator. A brass square 5.46 cm long and 0.33 cm thick was used as a surrogate TE generator and placed at the lens focus to collect solar energy. The experiment was conducted outdoors in a protected courtyard under direct sunlight. Brass target temperature was measured under a series of controlled convective heat transfer coefficients representative of ambient wind conditions. Additional recorded and measured parameters included absorbed thermal power, energy reflectivity index, and maximum temperature. Under concentrated flux, solar energy reflection from the target surface represents the most serious impediment to high temperature and improved TE efficiency. To reduce reflectance, the brass target was painted black. However, solar reflectance index only decreased from 93 ± 2 % for polished brass to 79 ± 2% for black-painted. At most, only about 20% of the available energy was collected. Under the best conditions, 398.1 ± 1.3 K was the highest target temperature recorded, corresponding to a TE generation potential of 0.5 watts. Surface reflectivity under concreted solar flux must be dramatically reduced to make TE a viable PV alternative in solar concentrating generators.

Nomenclature

α	=	coefficient of PV efficiency degradation with increased temperature
$\eta_{TE}[T_{TE,hot}]$	=	temperature-dependant energy conversion efficiency of a TE generator
$T_{TE,hot}$	=	TE generator hot end temperature
$T_{TE,cold}$	=	TE generator cold end temperature
z	=	thermoelectric figure of merit

[1] Research Assistant, Mechanical and Energy Engineering Department, 1155 Union Circle #311098 Denton, Texas 7603-5017, AIAA Student Member.
[2] Research Assistant, Mechanical and Energy Engineering Department, 1155 Union Circle #311098 Denton, Texas 7603-5017, AIAA Student Member.
[3] Assistant Professor, Mechanical and Energy Engineering Department, 1155 Union Circle #311098 Denton, Texas 7603-5017, AIAA Member.

I. Introduction

Our goal is to maximize thermoelectric (TE) energy generation on the sub-dekawatt scale using concentrated solar energy. An overwhelming volume of research, too much to capture in a few citations, has been done on large-scale systems for generating electricity using concentrated solar energy[1,2,3]; moderately less work exists for smaller scale systems. Nonetheless, professional research endeavors have studied solar concentration with Fresnel lenses on larger-scale photovoltaic (PV) systems,[4] while tiny Fresnel concentrator PV generators remain the province of hobbyists and researchers exploring indoor applications.[5] By limiting our attention to sub-dekawatt scale (less than 10-watt) concentrating solar collectors matched with PV, we noted two important limitations to power production efficiency. First, PV cell efficiency drops with increased temperature, yet concentrated sunlight focused on a solar cell drives its temperature up. Second, at some point a saturation limit is reached where PV cells produce no additional electrons even when photon flux is further increased; the photons are then either reflected away or absorbed as heat without producing power. These factors motivate use of a non-PV collector under concentrated sunlight; one that ideally is not impacted by the limitations of PV under highly concentrated light.

A heat engine would be ideal: efficiency increases as hot reservoir temperature rises, and the limit to photon flux capture occurs when power absorption is high enough to induce components to melt. Unfortunately, this solution proves too mechanically complex and expensive to be viable for sub-dekawatt power plants.[6] This analysis leads to thermoelectric (TE) generators as one viable option to fill this niche. TE's share the heat engine attribute of increased efficiency with higher collector temperature, but like PV cells they contain no mechanical parts. TE's are essentially sold-state heat engines that change thermal energy directly to electrical energy. Like conventional heat engines, TE generators operate across a temperature gradient. When the junctions of two different materials are maintained at different temperatures, a voltage is generated, which is directly proportional to the difference in temperatures. It is therefore advantageous to operate TEs under the largest possible temperature gradient to achieve the highest efficiency.

We are investigating the viability of a solar concentrating TE apparatus shown in Figure 1. The generator will be mounted on a metal pole sunk at least 12 meters into the ground, below the thermal inversion depth[7]. The deep ground will become a constant temperature heat sink for the TE cold end. The TE hot end will sit at the focus of a sun-tracking solar concentrator, which may be a single Fresnel lens, parabolic dish, or a combination of optics that keep sunlight focused on the generator throughout the day. This focusing mechanism will provide highly concentrated solar power flux and very high temperature to the generator.

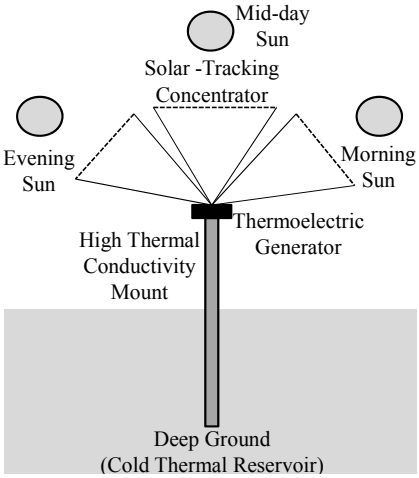

Figure 1. Schematic of the planned solar concentrating thermoelectric generator.

As a first step toward the design in Figure 1, we constructed an outdoor experiment that facilities control of many parameters important to attaining maximum temperature. Using a piece of brass as a surrogate TE generator we determined the maximum achievable temperature of the hot end. To heat the brass piece, a fixed Fresnel lens is used to create a focal point of sunlight directed at the brass. The lens is adjusted by hand as needed to keep the focus on target. Simultaneously, instruments deployed near the experiment measure ambient conditions to provide an estimate of the cold end temperature. Our experiment is designed to be self-calibrating in the field without use of expensive bench-top instruments. Transient warm-up and cool-down data yield solar flux density and convective heat transfer coefficient respectively. These parameters are compared to steady-state performance of the experiment as well as complimentary pyranometer data for validation.

II. Motivation and Background

PV cells become less efficient at higher operating temperatures, and utility-scale PV power installations have often use water cooling to maintain efficiency. As many utility-scale solar power plants are sited in desert areas where water is scarce, use of water for panel cooling and cleaning or as the working fluid in steam turbines has raised concern among environmentalists. For example, proposed projects in Nevada's Amargosa Valley would use 16.3 billion gallons of water per year from a nearby aquifer, enough to provide for 50,000 typical American homes. It is estimated that the basin in which the aquifer is located is capable of only providing half this water demand.[8] Air-cooled condensers could reduce the amount of water required for large scale solar projects, but this approach is less efficient than water cooled methods. Thus, more land would have to be used to build power plants at even

greater cost than water-cooled derivatives. [9] Solar power is already more expensive than conventional energy sources, and additional costs required to mitigate water use further reduce economic viability of this technology.

Cooling techniques have been demonstrated for PV arrays to maintain low temperature for improved efficiency. One technique even uses a siphon effect to eliminate parasitic pumping power (although municipal water pressure provides potential energy to initiate the siphon).[10] However, in remote locations where municipal water is unavailable and small power output on the order of 10 watts is adequate, parasitic energy consumption of available cooling techniques becomes an appreciable fraction of the generator output, reducing the practicality of cooling. Instead of battling against high solar collector temperature with a complicated cooling system, we propose to embrace it as an advantage.

In contrast to PV and steam turbine power plants, TE generators configured as shown in Fig. 1 will not consume any water. TE's can operate at elevated temperature for extended periods, and with no moving parts to wear out, they have maintenance-free lifetimes that exceed 100,000 hours (11.4 years).[11] Experts in the TE field have suggested that TE's show promise for solar energy generation under concentrated sunlight,[11] but with the expectation of studies involving exotic thermionic/thermoelectric conversion system,[12] practical applications are sparse.

III. Theoretical Modeling

We present three theoretical arguments in support of our experimental work. First, we apply the efficiency equations for a TE and a PV to demonstrate there exists an accessible temperature regime where TE efficiency exceeds PV efficiency. This conclusion motivates the second argument; we apply the first law of thermodynamics to idealized TE and PV generators under concentrated sunlight to show that the temperature regime where $\eta_{TE} > \eta_{PV}$ is consistent with sub-dekawatt scale generators. Third, we introduce an analytical model for the experimental apparatus described below, which allows us to benchmark the performance and validity of our experiments.

A. Efficiency Comparison for TE and PV Generators

The temperature-dependant energy conversion efficiency of a TE generator, $\eta_{TE}(T_{TE,hot})$, depends upon three parameters: the hot end temperature, $T_{TE,hot}$; the cold end temperature, $T_{TE,cold}$; and the thermoelectric figure of merit, z.

$$\eta_{TE}\left[T_{TE,hot}\right] = \frac{\left(T_{TE,hot} - T_{TE,cold}\right)}{T_{TE,hot}} \frac{\sqrt{1 + z\left(\frac{T_{TE,hot} + T_{TE,cold}}{2}\right)} - 1}{\sqrt{1 + z\left(\frac{T_{TE,hot} + T_{TE,cold}}{2}\right)} + \frac{T_{TE,cold}}{T_{TE,hot}}} \tag{1}$$

For this analysis we assume the cold end of the TE is in perfect thermal communication with a cold reservoir at $T_{TE,cold}$ = 300 K, approximately ambient temperature. To provide this thermal reservoir in the real system we plan to build, the cold end of the TE generator will be affixed to a thermally conducting metal rod. The rod will be sunk deep enough to use the ground as a thermal sink. We approximate z = 0.0013 1/K, which is an empirical value for Bi_2Te_3 thermoelectric material under a 88.1 K temperature gradient at a mean temperature of 322 K.[13] We intentionally selected a z value lower than conventionally reported for thermoelectric material because our TE will experience a large temperature gradient, and Min, Rowe, and Kontostavlakis report degradation in z under this condition. We further assume that z is not a function of temperature.

The coefficient of efficiency degradation with increased temperature for silicon PV, α, is between -0.003 %/K and -0.006 %/K from a reference temperature of 300K.[14] To provide the most favorable case for PV efficiency, we assume α = -0.003 %/K, and that it is not a function of temperature. Field deployed flat plate single crystalline silicon PV modules have a maximum measured efficiency not exceeding 12%.[15] Combining these empirical parameters into an equation of PV efficiency as a function of temperature gives.

$$\eta_{PV}\left[T_{PV}\right] = 0.12\left\{1 + \alpha\left(T_{PV} - 300\right)\right\} \tag{2}$$

Equations 1 and 2 are not complete phenomenological models, and they perhaps oversimplify the temperature-dependant behaviors of the materials they represent. These models nonetheless motivate the underlying assertion of this research: at high collector temperature, TE efficiency exceeds PV efficiency.

B. Energy Balance for Solar Generators under Concentrated Sunlight

To estimate the size of a system that achieves the efficiency crossover temperature of 495 K, the ratio of solar concentrator to solar generator area, A_{lens}/A_{TE}, is needed. We apply the first law of thermodynamics to a control volume containing the TE solar generator system portrayed schematically in Figure 2. We make the following assumptions: 1) the system cannot store energy and is operating at steady state; 2) unless otherwise noted, variables are not functions of temperature; 3) the spatial temperature across the hot side of the system is uniform; 4) all sunlight that strikes the concentrating lens is focused onto the TE generator; 5) ambient temperature, T_∞, and the temperature on the cold side of the TE generator, $T_{TE,cold}$, are fixed at 300 K; 6) no heat is lost through the TE generator by conduction through the cold side; 7) the system is enclosed on all sides, except the exposed face, with an adiabatic boundary; 8) the system has a uniform reflectivity, ρ, on its exposed surface; 9) the exposed face of the collector exchanges heat via forced convection with air blowing over this surface. We estimate the average forced convection coefficient, h = 21.7 W/m^2-K. This value is obtained from a correlation for laminar flow over a flat plate[16] 10 cm long under a constant air velocity of 3 m/s. The resulting equation is

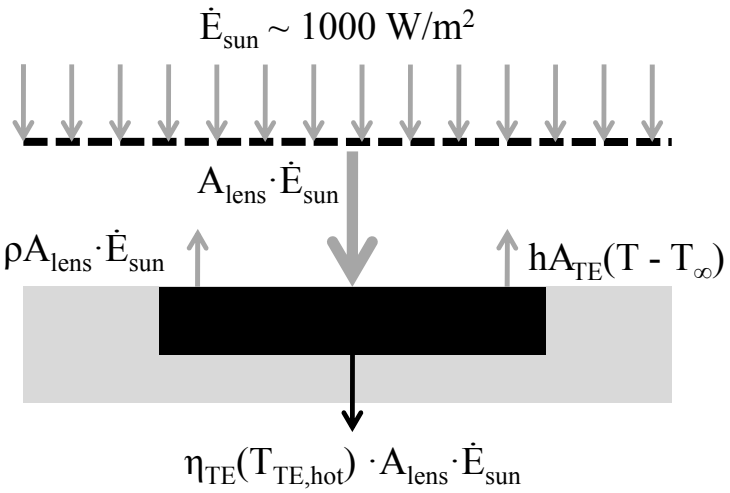

Figure 2. An energy flow accounting model for a TE generator running under concentrated sunlight.

$$0 = A_{lens}\dot{E}_{sun} - \rho A_{lens}\dot{E}_{sun} - hA_{TE}\left(T_{TE,hot} - T_\infty\right) - \eta_{TE}\left[T_{TE,hot}\right]A_{lens}\dot{E}_{sun} \tag{3}$$

where A_{lens} and A_{TE} are respectively the areas of the concentrating lens and TE generator, $\dot{E}_{sun}$ is solar energy flux density, ρ is the surface reflectivity, h is the forced convection coefficient, $T_{TE,hot}$ and T_∞ are respectively the temperatures of the TE hot side and the ambient environment, and $\eta[T_{TE,hot}]$ is the TE generator efficiency as a function of the TE hot side temperature (expressed in Eq. 1). Rearranging Eq. 3 to solve for A_{lens}/A_{TE} gives Eq. 4.

$$\frac{A_{lens}}{A_{TE}} = \frac{h\left(T_{TE,hot} - T_\infty\right)}{\dot{E}_{sun}\left(1 - \rho - \eta_{TE}\left[T_{TE,hot}\right]\right)} \tag{4}$$

We note that the simplifying assumptions, especially (6) and (7), yield a lower bound on the ratio A_{lens}/A_{TE} because they eliminate paths of thermal energy leakage that would be present and appreciable in the real system. However at the efficiency crossover temperature $\eta_{TE} \sim \eta_{PV}$, PV generators do not require heat conduction from a cold end for proper operation. Therefore Eq. 4 provides a reasonable A_{lens}/A_{TE} design threshold for concentrating solar energy systems beyond which use of a TE generator should be considered in place of a PV generator. Using parameters listed in Table 1 and the efficiency crossover temperature $T_{TE,hot}$ = 495 K the ratio A_{lens}/A_{TE} = 4.7.

Table 1. Parameter values applied to solution of Eq. 4.

Parameter	$T_{TE,hot}$	$T_{TE,cold}$	T_{oo}	z	h	$\dot{E}_{sun}$	ρ
Units	[K]	[K]	[K]	[1/K]	[W/m^2-K]	[W/m^2]	[ ]
Value	495	300	300	0.0013	21.7	1000	0.05

Given the analytical guidance developed here, we designed and built an experimental apparatus whose performance closely matches the assumptions and parameters underlying Eq. 4 to validate our modeling approach.

C. Analytical Model of Experimental Apparatus

We model thermal performance of a system under concentrated sunlight using a lumped mass control volume containing only the target material. The material does not change phase and its specific heat is not a function of temperature. This control volume is thermally insulated on all external surfaces, except the upward facing surface, with a perfect adiabatic boundary. The upper surface receives a spatially uniform flux of solar energy, and a portion of this energy is absorbed and a part reflected. The reflectivity of the exposed surface is completely uniform. The upper surface also experiences forced convective heat transfer to a stream of air arriving at ambient temperature. Regardless of the system temperatures, natural convection is assumed negligible compared to forced convection and is ignored. The first law of thermodynamics applied to this lumped parameter model gives the following expression.

$$(1-\rho)\dot{E}_{sun}A_{lens} = hA(T - T_{\infty}) + mc\frac{\partial T}{\partial t} \tag{5}$$

Different operating conditions applied to Eq. 5 enable measurement of important experimental parameters. In the early period of the warm-up transient from ambient temperature, the convective heat transfer term is negligible provided $T \sim T_{\infty}$, and in this special case, Eq. 5 becomes the following:

$$(1-\rho)\dot{E}_{sun}A_{lens} = mc\frac{\partial T}{\partial t} \tag{6}$$

If the mass and specific heat of the target material are known, then measured temperature change with time gives the energy absorbed by the target material. The experiment effectively becomes a pyranometer for measurement of its own absorbed solar energy. Moreover, if the total solar energy flux is independently measured, Eq. 6 can be solved for the solar spectrum reflectivity of the target material.

When steady-state conditions are achieved at elevated temperature, the temperature derivative with respect to time vanishes to zero: $\partial T/\partial t \to 0$. Under these conditions, Eq. 5 becomes the following.

$$(1-\rho)\dot{E}_{sun}A_{lens} = hA(T - T_{\infty}) \tag{7}$$

The absorbed solar energy, determined from experimental measurements and Eq. 6 is known. Ambient temperature and the target material temperature are also known. Thus, Eq. 7 can be solved for the forced convection coefficient. Finally, when the experiment cools down, solar energy is no longer being absorbed by the target material. Eq. 5 can be recast and integrated into the following form.

$$T(t) = (T_{high} - T_{\infty})e^{-\frac{hA}{mc}t} + T_{\infty} \tag{8}$$

Eq. 8, the classic Newtonian cool-down expression serves to independently verify the experimentally measured forced convection coefficient obtained using Eq. 7. These equations enable analysis and evaluation of the performance of our experimental system for comparison to the idealized analytical model described by Eq. 3.

IV. Methods

A. PV Maximum Power Point Determination

The PV output power shifts as the load across it changes. Large PV installations use automatic maximum power point (MPP) trackers that adjust the direct current load resistance as conditions change to maximize the power derived from the PV. MPP trackers consume power parasitically, but the loss is more than made up by the extra power production MPP's enable in large PV arrays. However, this parasitic power loss overwhelms small installations, (especially in the range below 10 watts of interest in this paper).

The direct current resistive load that gave the MPP for our PV panel at 300 K was found experimentally and used for all the later experiments. We note that the MPP load at room temperature may not correspond to the MPP load at elevated temperature. However, as MPP for an installed sub-deki-watt system will likely not be adjusted automatically, we chose to use the resistance for room temperature MPP as the representative, fixed value.

A Radio Shack 25 Ω three terminal rheostat was wired across the leads of the PV cell. The ammeter function of a PASCO Data Studio PASPORT power sensor was wired in series with the rheostat, and the sensor's voltmeter function was wired in parallel with the rheostat. Across the rheostat central lead and its unused terminal was attached a Cen-Tech pocket digital multimeter in resistance meter mode. Before the experiment, the total rheostat resistance was measured to be 25.1 Ω. This wiring arrangement enabled determination of the resistance applied to the PV cell by subtracting from 25.1 Ω the resistance meter reading.

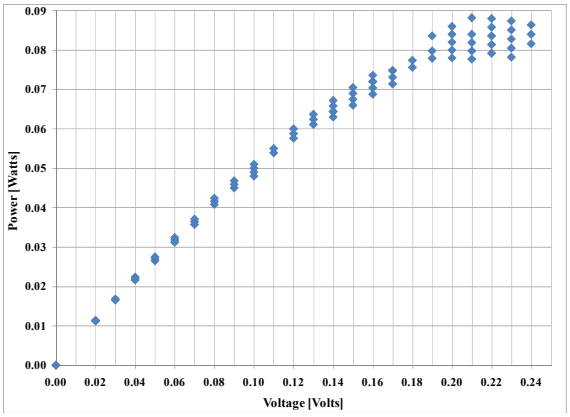

Figure 3. Experimental PV cell power-voltage curve shows the MPP at 0.22 volts and 0.42 amps, which corresponds to a load of 2.5 Ω.

A Solar World 4-600 solar cell was removed from its encapsulation module and set up 70 cm from a Newport 67005 sun lamp with an Oriel 62020 light filter; the sun lap was powered by a Newport 69911 power supply, which was set at 160 watts for this experiment. With PASCO Data Studio logging voltage across and current through the rheostat, its resistance was slowly decreased across is full range. The resulting power-voltage curve for the PV cell is given in Fig. 3, and the MPP corresponds to a rheostat setting of 2.5 Ω, which gave 0.22 volts at 0.42 amps.

B. Solar Flux Data for Denton, TX

A literature search revealed that instantaneous solar flux for Denton, TX was not available. To create this data for a typical cloudless Denton spring day, an Apogee SP-110 pyranometer was placed on a residential rooftop above the tree and building levels in the area to eliminate shadowing. Pyranometer output was logged once every 30 seconds using the voltmeter setting of an Extech 380900 multi-meter. Logging occurred for a full 36 hours, starting in the afternoon of April 22, 2009 with the sun directly overhead and ending the next evening. A solar flux curve for a full day, shown in Figure B, was captured as was as the lunar flux curve for the evening of April 22, 2008.

Some of the data presented in the Results section was taken before a pyranometer was available for instantaneous solar flux monitoring. For these experiments, we describe assumptions including fixing the solar flux at 1000 w/m^2 when the sun is directly overhead. The data for Fig. 4 show that this assumption was valid.

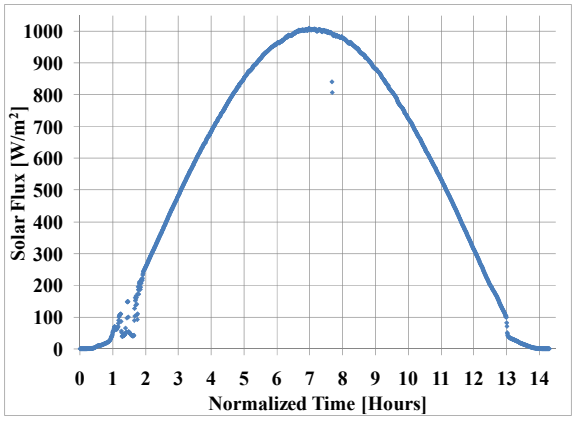

Figure 4. Instantaneous solar flux on a near-cloudless Denton, TX day taken on April 22, 2009.

C. PV Efficiency Degradation at Elevated Temperature

To measure the PV efficiency degradation at elevated temperature, a Solar World 4-600 PV cell (removed from its encapsulation module) was used. The PV cell was affixed to a Provocraft Candlscense residential candle warmer using temperature resistant RTV adhesive. AC power to the candle warmer as controlled with a Proformax SRV-10 Variac transformer whose voltage output was monitored by an Extech MultiMaster^{TM} 570 true RMS multimeter. Temperature at the PV cell was adjusted by varying the variac power output to the candle warmer.

The PV-heater assembly was arranged to hang vertically and placed 38 cm from the Newport 67005 sun lamp with Oriel 62020 filter lens and Newport 69911 power supply. The sun lamp power supply was set to output 160 Watts throughout the experiment, corresponding to a solar flux of 960 ± 10 w/m^2. The solar flux was never changed in this experiment to ensure that the efficiency degradation with temperature was isolated from degradation related to photon saturation. The solar flux was determined after the experiment by placing an Apogee

SP-110 pyranometer at the same distance from the sun lamp that the PV cell was located and measuring output with an Extech 380900 logging multi-meter.

During the experiment, the instantaneous temperature of the PV cell was measured using a single Omega Engineering 5SC-TT-K-40-36 K-type thermocouple affixed to the center of the cell on the exterior face with high-temperature-resistant electrical tape. The fixture point and thermocouple wire path running away from the assembly was co-located along on the PV cell metal pick-ups so no photons incident on an active collector surface were blocked. The thermocouple was monitored with an Omeag OM-2041 portable data logger, and the PV cell voltage and current output were monitored using an Extech 380900 logging multi-meter. A rheostat set to 2.5 Ω (the room temperature MPP load) was wired across the PV cell to provide a constant electrical load, which as continuously measured via a Cen-Tech pocket digital multimeter in resistance meter mode.

The experiment was started by shining the sun lamp directly on the PV cell, turning the heater to output 100.3 VAC, and allowing the PV cell to warm to 380.3 K. under these conditions, the temperature was allowed to settle. Steady temperature was defined throughout this experiment as the condition in which the measured PV temperature remained within 1 K of an observed temperature for 360 seconds. After recording data at each steady-state set point, the heater voltage was reduced nominally 10 VAC and the system allowed to settle to a new steady state temperature.

The experiment was conducted in the cool-down direction from a high voltage of 100.3 VAC to the low voltage of 0.0 VAC. The experiment was repeated in the heat-up direction starting at 5.15 VAC and increasing in nominal increments of 10 VAC. Two different temperature directions were used to determine if there was any dirction-dependant hysteresis in the measurement but no hysteresis effect was found.

D. PV Efficiency Degradation at Elevated Photon Flux

To experimentally capture the PV photon saturation limit, a Solar World 4-600 PV cell (within its encapsulation module, but with the concentrating lens cover removed) was fixed to the flattened face of a metal coffee can with duct tape. PV cell voltage and current output were monitored using an Extech 380900 logging multi-meter. A rheostat set to 2.5 Ω (the room temperature MPP load) was wired across the PV cell to provide a constant electrical load, which as continuously measured via a Cen-Tech pocket digital multimeter in resistance meter mode.

The assembly was placed 70 cm away from a Newport 67005 sun lamp with Oriel 62020 filter lens using a Newport 69911 power supply. The sun lamp power supply was first set to output 160 watts, corresponding to a solar flux of 525 ± 10 w/m^2, below the PV photon saturation point, and the temperature was allowed to settle to steady-state. Over the course of the experiment, the sun lamp power output was increased in increments of 10 watts up to 390 watts, corresponding to a solar flux of 1453 ± 10 w/m^2; at this setting the sun lamp itself overheated and performed an automatic shut-off. The solar flux corresponding to each sun lamp power supply set point was determined after the experiment by placing an Apogee SP-110 pyranometer at the same distance from the sun lamp that the PV cell was located and measuring output with an Extech 380900 logging multi-meter.

To ensure the photon saturation experimental results were isolated from efficiency degradation with increasing temperature, a single Omega Engineering 5SC-TT-K-40-36 K-type thermocouple was affixed to the center of the PV cell housing module on the duct-taped face abutting the coffee can. The thermocouple was monitored with an Omega OM-2041 portable data logger. To keep the PV cell temperature constant despite increasing solar flux, The metal coffee can to which it was affixed was flattened and filled with ice and water. A pin hole was made on the can's bottom drain water (and carry away heat). As ice melted and drained, more ice and water were added to the can to keep the PV isothermal. As an additional measure, a high-speed fan was directed over the PV cell to convect away heat. These measures succeeded in keeping the PV cell temperature between 290.4 K and 300.5 K. From our temperature degradation data to characterize this PV cell, we expect a loss in total efficiency no greater than 0.23% owing to the slight increase in temperature as solar flux was increased almost 3-fold.

E. Solar Collection Experiment at a 28.8:1 Concentration Ratio by Area

For these experiments, a square piece of Alloy 385 brass 5.46 ± 0.01 cm long by 5.46 ± 0.01 cm wide, 0.33 ± 0.01 cm thick and 77.3111 ± 0.001 g in mass was used as the surrogate thermoelectric generator. In the first set of experiments, the brass surface was polished with 60-grit sandpaper. In the second set of experiments, the polished surface was painted over with one coat of Golden Acrylics "Carbon Black" paint (Golden # 1040-4) in an effort to make the surface less reflective.

A single Omega Engineering 5SC-TT-K-40-36 thermocouple was soldered to the underside center of the brass square. This thermocouple type is made with 40 AWG wire, the smallest commercially available readymade thermocouple, and it was chosen to minimize surface temperature measurement errors arising from the presence of the thermocouple on the brass as well as the thermocouple fin effect. Manufactured using "special limits or error"

material, the thermocouple experimental error was ± 1.1 °C. The temperature data was sampled at 1 Hz for the unpolished brass experiment and 0.0167 Hz for the black-painted brass experiment and recorded using an Omega Engineering OM-2041 portable data logger. The measurement error in the logger is ± 0.7 °C for the temperature range of interest. Propagation of experimental error yields a measurement uncertainty no greater than ± 1.3 °C. Using the highest forced convection heat transfer coefficient experimentally measured (h = 71 W/m^2-K, described below), the Biot number through the brass in the thickness direction was 0.002 while in the width direction, it was 0.035. We therefore assume spatial temperature uniformity across the brass, which is measured by the affixed thermocouple.

The brass is mounted in an insulating ceramic support with the thermocouple facing downward (Fig. 5). A square crevice 0.33 cm deep was chiseled into the ceramic so the brass square lays flush with the surface of the ceramic. The textbook thermal conductivity of the ceramic is 0.72 W/m-K, and it is at least 1.07 ± 0.01 cm thick in all directions surrounding the bass square. Neglecting the contact resistance (which provides additional thermal insulation) the thermal conductance through the ceramic is at least kA = 0.012 W/K. The lowest experimentally measured thermal conductance due to forced convection over the brass plate (hA = 0.113 W/m^2-K, described below). By comparing the conductance of the ceramic insulator to forced convection, at most only 10.7% of the heat leak from the brass square can be attributed to conduction through the ceramic. We therefore assume that the ceramic provides an adiabatic barrier to conductive heat transfer and all heat loss from the brass square is via forced convection from its exposed surface.

Figure 5. Small-Area Fresnel solar concentrator apparatus with the brass target unpainted (left) and painted black (right). These images show the marked difference in energy reflectance realized between these two surface treatments.

Air velocity, air temperature, and relative humidity over the brass square and ceramic insulator are measured with a Kestrel 4000 pocket wind meter mounted with its anemometer fan 12 ± 1 cm from the leading edge of the ceramic support and 9 ± 1 cm from the leading edge of the brass square. Data were recorded at 0.2 Hz, and the instrument's velocity, temperature, and relative humidity measurement uncertainties are ± 0.1 m/s, ± 1.0 °C, and ± 3.0% RH respectively. Ambient temperature and relative humidity are measured with an Extech 310 logging hygrometer at a sampling rate of 0.1 Hz. The experimental uncertainty in temperature and relative humidity are ± 0.7 °C, and ± 2.5% RH respectively. The logging hygrometer is placed at least 2 meters from the experiment, in the shade, off the ground on a plastic-insulated bench to ensure accurate ambient readings beyond any interference from the experiment.

The solar concentrating lens is a 29.3 ± 0.5 cm x 29.3 ± 0.5 cm square Fresnel lens scavenged from a 3M 910 Lamp Changer overhead projector. The lens is mounted on a pair of ring stands and situated over the brass square facing the sun so the concentrated solar focal point is targeted on the center of the brass square. Forced convection over the experiment is provided by a commercial-off-the-shelf rotary fan with three qualitative settings: low, medium, and high. The face of the fan is situated coincident with the leading edge of the insulating ceramic, and the axis of the fan is offset from the brass square to the edge of the blades are visually aligned with the edge of the brass square. This arrangement exposes the brass square to the portion of the fan wake near the edge of the blades where the wind velocity is highest.

The experiment is situated at the approximate center of a 22.9 m by 5.49 m rectangular courtyard enclosed on all sides with the exception of an 11.9 m wide walkway approaching from the south. The surrounding building is at least 5.5 m tall and shields the courtyard (and the experiment) from wind. The experiments using unpainted,

polished brass as the solar target were conducted on March 11, 2008 from 11:25 am to 1:47 pm. The experiments using black-painted brass were conducted on September 15, 2008 from 11:41 am to 1:32 pm. Both days were selected because the sky was cloud free and represented typical Texas weather. Moreover, the March date closely coincided with the March 20, 2008 vernal equinox while the September date closely coincided with the September 22, 2008 autumnal equinox. Juxtaposed against solstices when ambient temperatures are at extremes, equinoxes are beneficial for temperature-dependant solar experiments because are more representative of average year-round ambient conditions. The choice to test between 11:00 am and 2:00 pm also mitigated swings in ambient temperature and solar flux during the experiments because variation in these parameters during this time block is less severe than earlier or later in the day.

Both sets of experiments, with unpainted brass and black painted brass, follow the same standard operating procedure. With a sunlight blocker in place, all logging instruments were started simultaneously. The fan was set running first at its "low" setting, and the experiment was allowed to thermally settle for at least ten minutes. At an integer logging interval, the sunlight blocker was removed to instantaneously expose the brass square to concentrated sunlight from the Fresnel lens. The brass square heated up and was allowed to settle to a new steady-state temperature. We define steady state as an elevated temperature that does not fluctuate more than 7.0 °C for 5 minutes. After the 5-minute steady state period is complete, the sunlight blocker is replaced at an integer logging interval, and the brass square undergoes Newtonian cool-down, returning to ambient temperature. Once 5 minutes elapse with the shielded brass square at ambient temperature, the fan velocity is increased to the next setting, "medium", and the process is repeated. The process is repeated once more with the fan set to "high". At the conclusion of the experiment all logged data is uploaded to a PC for processing and analysis.

F. Solar Collection Experiment at a 275:1 Concentration Ratio by Area

To find the maximum temperature that a thermoelectric generator could be heated to, a brass piece was used as a surrogate TE generator (Fig. 6). Two experiments were run, one with an uncoated brass piece and a second with 3 coats of Krylon BBQ & Stove paint, which leaves a dull black finish and withstands temperatures up to 1200 °F (922 K). The experiments were exact in every other way.

A 104.1 cm by 78.7 cm rectangular Fresnel lens was mounted in a wooden frame above two bicycle wheels that allowed for forward and backward rotation of the lens (Fig. 7). These wheels were mounted to a large surface that swiveled 360 degrees. Attached to this surface, under the Fresnel lens was a brick piece with a square cut into it to allow the brass piece to sit flush with the surface. A high temperature Omega Engineering WTK-6-24-SMPW-M K-Type thermocouple was screwed into the brass piece. Enough slack was left on the wire to allow for expansion from heat, and it was fed back to a thermocouple reader that was mounted to the large surface out of the sun.

To measure the solar flux, a pyranometer was mounted to the frame holding the Fresnel lens so that it would always be at the same angle as the sun as he lens. Wires were connected from the pyranometer to the multimeter which was mounted near the thermocouple reader. A fan was set up with a turbulence breaker to blow air over the brass piece. A Kestrel 4500 weather station was set up a few feet away from the Fresnel lens contraption to measure ambient conditions.

The multimeter was set to log every second in mV DC. The thermocouple reader was set to log every 2 seconds for a logging time of 5 hours in degrees Celsius. The Kestrel weather station was set to log every 2 minutes. All the instruments were cleared before the start of the experiment. The flash point of the Fresnel lens was found and lined up with the brass piece. Then the Fresnel lens was blocked completely. All the instruments were started simultaneously and allowed to run for five minutes. The fan speed was

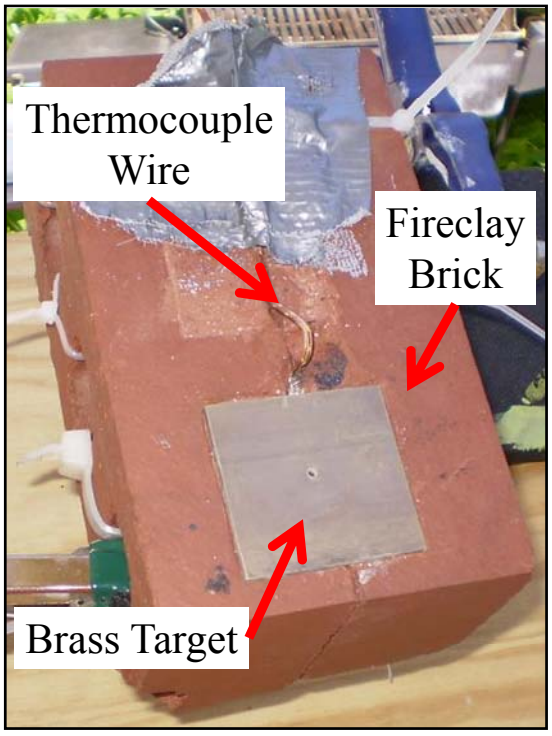

Figure 6. Ceramic mount that held the brass target in place under the large-area Fresnel concentrator. A K-type thermocouple bead was mechanically affixed to the bottom of the target, and its protruding wire was kinked to prevent thermal expansion from unseating the brass from the ceramic as the assembly warmed up.

started on high. Then the Fresnel lens was unblocked and the focal point was set on the brass piece over the thermocouple on the underside. Throughout the experiment the focal point was adjusted to remain in the center of the brass piece. As soon as the brass piece reached its maximum temperature, the Fresnel lens was recovered and the brass piece was allowed to cool on its own, thereby capturing the convection coefficient. This process was repeated through three fan speeds.

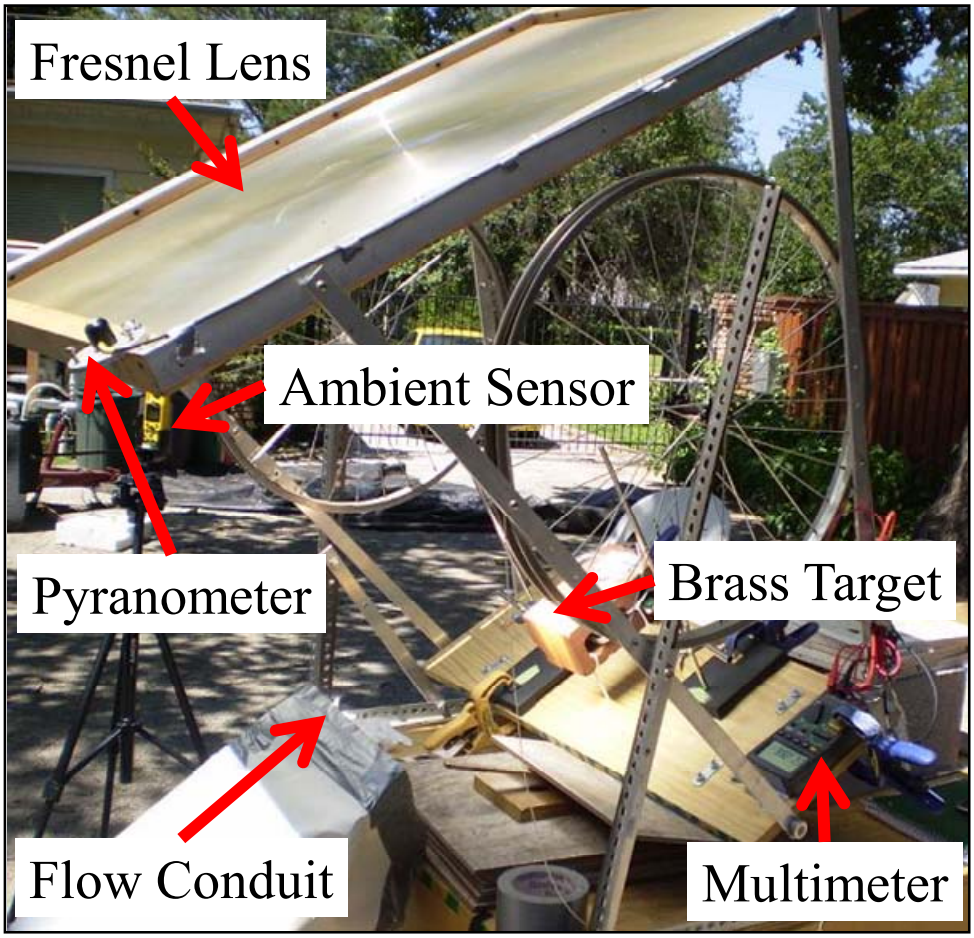

Figure 7. Large-Area Fresnel solar concentrator apparatus showing all the components used to regulate conditions and take data.

V. Results and Analysis

A. PV Efficiency Degradation at Elevated Photon Flux

The photon flux saturation flux data is shown in Fig. 8. This data is represented by the available solar flux density increasing along the X-axis while the measured response in PV solar output indicated on the Y-Axis. It was expected that as available solar flux increased, a proportional increase in PV output would be observed. As the ability of the PV cell to absorb additional photons became saturated, the output was expected to gradually flatten out, indicating that no additional power was being generated despite availability of additional elections. The temperature of the PV should also have been observed to increase as photons that would previously have been converted to electricity were instead converted to heat.

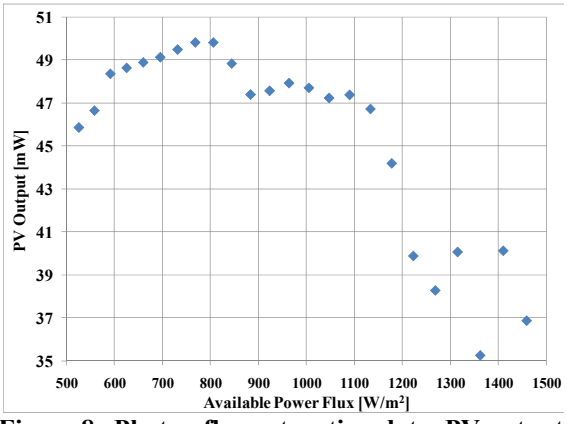

Figure 8. Photon flux saturation data. PV output increases with available flux, plateaus at 1100 w/m^2, and then drops at higher flux rates.

The observed result in Figure 8 was not consistent with the expected behavior. PV output did increase with solar flux, and it appeared to begin a plateau at 800 w/m^2 of solar flux. However, the output dropped slightly around 900 w/m^2 solar flux, and then appeared to establish a second plateau until solar flux reached around 1100 w/m^2. Despite attempts to keep the PV cell isothermal, it is possible that the drop in PV output at 900 w/m^2 solar flux is associated with increasing cell temperature as photon saturation was reached. However, the precipitous drop in PV power output above 1100 w/m^2, a reduction of over 28%, remains unexplained. This experiment will have to be carefully repeated before meaningful conclusions can be drawn.

B. PV Efficiency Degradation at Elevated Temperature

Equations 1 and 2 are plotted in Figure 9, showing the energy collection efficiency of TE and PV generators verses collector temperature. The figure shows that as collector temperature increases above ambient, TE efficiency improves from 0% while PV efficiency decreases from 12%. Near a collector temperature of 495 K, these two efficiency curves cross at approximately 5% and additional temperature increase further improves TE efficiency. While not in the range of Figure 9, it is also noteworthy that at temperatures exceeding 830 K, TE efficiency exceeds the base PV efficiency of 12% at 300 K.

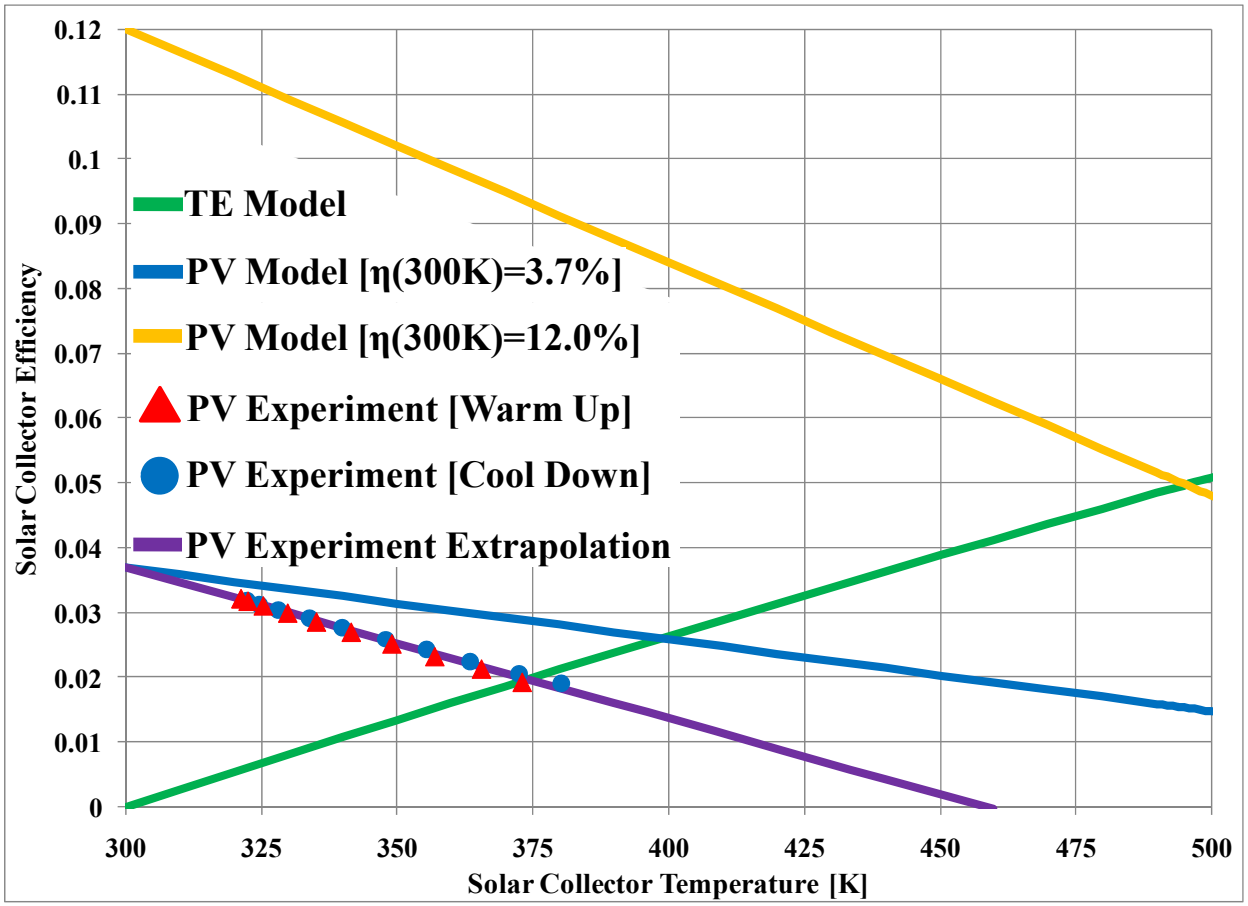

Figure 9. Efficiency curves for a variety of PV and TE models. Equation 1 (for TE) is presented in green and Equation 2 (for PV) is given in yellow. These curves represent textbook models using textbook performance parameters for these generators. Their crossing, 495 K, is the temperature at which TE efficiency exceeds PV efficiency under identical conditions. Experimental PV output degradation with temperature is shown using data points of red (for heat-up) and blue (for cool-down). Extrapolating these data to 300 K (the purple curve), indicates the PV room temperature efficiency is 3.7% instead of 12% reported in the literature. The crossing between these data and the TE model suggests that TE becomes more efficient than PV above 375 K. Finally, the blue curve represents the PV model in Equation 2, but with 3.7% efficiency at 300 K. The TE curve efficiency crossover temperature for this PV model is 400 K.

C. Solar Collection Experiment at a 28.8 Concentration Ratio by Area

Figure 10 shows the time-temperature histories for both unpainted and painted brass target solar concentrator experiments using matched temperature scales for emphasis. Recorded peak temperatures for each fan velocity setting (i.e., each convection coefficient, h1, h2, and h3) are denoted on the figure. The warm-up, steady-state, and cool-down data from all six runs are applied to Eqs. 6 – 8 to calculate convection coefficient, power absorbed, and the reflectivity index for each test.

Table 2 reports measured and calculated experimental parameters. The peak temperature for each experiment is the maximum temperature recorded by the thermocouple affixed to the brass target during the steady state period of each test. The qualitative fan speeds are buttressed by quantitative measurements taken by the Kestrel 4000 anemometer placed downstream of the brass target. The reported velocities are averaged values of discrete data points taken over the duration of each test. The reported experimental uncertainties in velocities are standard deviations of the data about the averages. Substantial velocity differences between identical fan settings along with large experimental uncertainties in the resulting values suggest that air velocity over the brass target is very sensitive to the spatial location of the experiment within the fan wash. Future experiments will improve the consistency of air velocity delivery using a wind trough to capture all the fan flow and direct it over the brass target. A turbulence breaker will also be used to reduce vortices and instabilities in the flow. The challenge is building trough that does not shadow the brass target or optically interfere with the focus path from the Fresnel lens. Thus, this component was not included in the initial series of experiments.

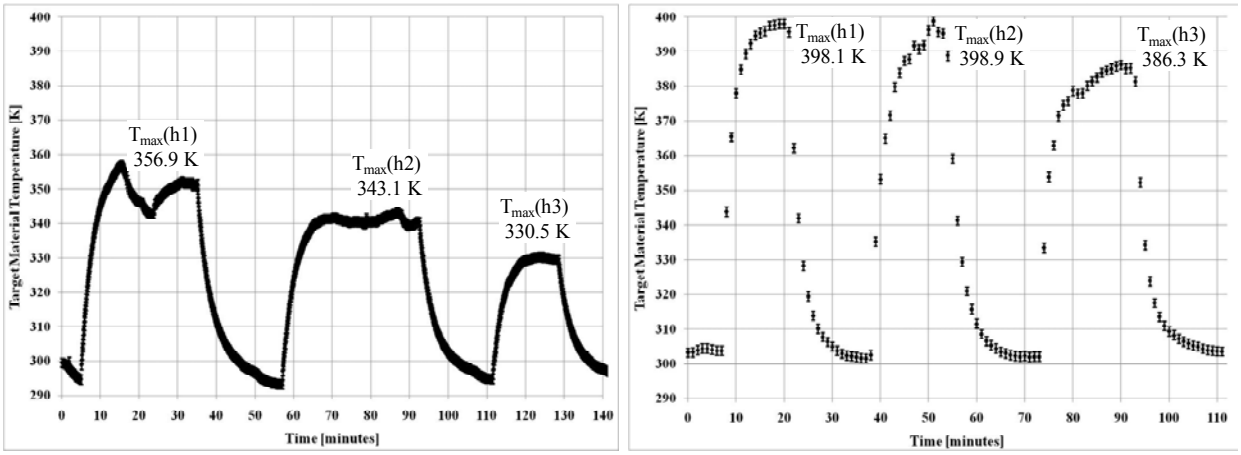

Figure 10. Temperature-time histories for unpainted (left) and black painted (right) brass targets under concentrated sunlight at three different qualitative fan velocity settings: low, medium, and high. Reduced reflectivity index owing to painting the target surface back yields increased energy absorption, which manifests as increased target temperature.

Table 2. Measured and calculated experimental parameters of a brass target under concentrated sunlight.

Target	Unpainted Brass			Painted Brass		
Max Temp [K]	356.9	343.1	330	398.1	398.9	386.3
Fan Setting [ ]	Low	Medium	High	Low	Medium	High
Ave. Vel [m/s]	0.72 ± 0.18	1.27 ± 0.23	1.35 ± 0.20	2.56 ± 0.57	3.15 ± 1.08	3.63 ± 1.12
h [W/m2-K]	38	40	48	68	63	71
Power Absorbed [W]	6.6	5.7	4.8	19.4	17.6	17.4
Generation Potential [W]	0.10	0.07	0.04	0.50	0.46	0.40
ρ (Ėsun = 1000 W/m^2) [%]	92	93	94	77	80	80

VI. Conclusions

Our key finding is that the reflectances of the surfaces we placed under concentrated sunlight limited the thermal power absorption of the brass targets used as TE surrogates. Despite minimizing the surface reflectivity by coating the target material with black paint, about 80% of the incident energy was reflected away, and it was therefore not available to increase temperature (and thermodynamic efficiency) and be converted to electricity. Moreover, under high solar flux generated with the large-area Fresnel lens, acrylic-based paint burned off, forcing a switch to Stove and BBQ paint (Fig. 11). Of the two surface treatments, the acrylic paint had lower reflectivity and hence better performance. A surface treatment with low reflectivity that can withstand high heat must be identified to increase energy conversion efficiency of TE generators under concentrated sunlight.

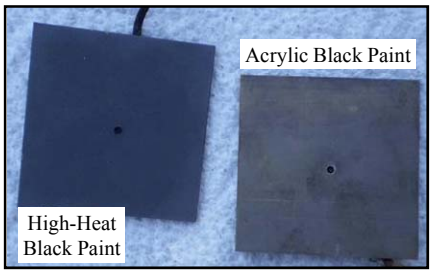

Figure 11. High solar flux exposure burned off acrylic-based paint (right), while BBQ & Stove paint (left) survived. Surface treatments with low reflectivity that can withstand high heat are needed to improve efficiency.

Even given surface treatment limitations, we showed experimentally that a surrogate TE generator hot end under concentrated sunlight can be increased above the efficiency crossover temperature of 375 K for the PV cell studied. Under these conditions, we expect TE to outperform PV. Thus, this technique shows promise for future investigation leading to sub-deka-watt scale solar concentrators coupled with TE generators for remote power production. These generators require no water for cooling or cleaning and, in fact, run at increased efficiency in the absence of coolant.

Acknowledgments

This work was supported by the Mechanical and Energy Engineering Department and the College of Engineering at the University of North Texas through the Researcher Incubator, a training organization to fast-track undergraduate students into engineering research experiences. The authors acknowledge Steve Morriss of Denton, TX, who sponsored a portion of this research and served as an industry mentor for the student researchers. We also acknowledge UNT students Jared Fiorentine and Joshua D. McNutt for assisting with data collection with the large-area Fresnel experiment and the small-area Fresnel experiment, respectively.

References

1 Stone, K. W., Garboushian, V., Markarian, K., Wood, G., Boehm, R., Hurt, R., Gray, A., Haydan, H., and Fletcher, T., "Installation and Operation of the Amonix High Concentration PV System at Nevada Power Company in Las Vegas, Nevada," 2006, IEEE 4th World Conference on Photovoltaic Energy Conversion, May 7-12, 2006, Hilo, Hawaii.

2 Halford, M. C., and Boehm, R., "Simulation and Optimization of a Concentrated Photovoltaic System," Journal of Solar Energy Engineering, May 2006, pp. 139-145.

3 Rabl, A., and Winston, R., "Ideal concentrators for finite sources and restricted exit angles," Applied Optics, Vol. 15, 1976, pp. 2880-2883.

4 Kritchman, E. M., Friesem, A. A., and Yekutieli, G., "Highly concentrating Fresnel lenses," Applied Optics. Vol. 18, 1979, pp. 2688-2695.

5 Hande, A., Polk, T., Walker, W., Bhatia, D., "Indoor solar energy harvesting for sensor network router nodes," Microprocessors and Microsystems, Vol. 31, 2007, pp. 420–432.

6 McNutt, J. D., Fallwell, C. M., Traum, M. J., "Assessing Energy Conversion Efficiency for Sub-Kilowatt Thermoelectric Generators Under Concentrated Sunlight," University Scholars Day 2008, University of North Texas (UNT), Denton, TX April 3, 2008.

7 Boyle, G., Renewable Energy, 2nd Ed., Oxford University Press, 2004, Figure 9.12.

8 Beamish, R., "Going solar makes it difficult to go green for company," Contra Cost Times [on-line newspaper article], April 18, 2009, URL: http://www.contracostatimes.com/ci_12175497?source=most_viewed, [cited 15 June 2009].

9 Maloney, P, "Solar Projects Draw New Opposition," New York Times, [on-line newspaper article], September 24, 2008, URL: http://www.nytimes.com/2008/09/24/business/businessspecial2/24shrike.html?pagewanted=print, cited 15 June, 2009].

10 Kaoru Furushima and Yutaka Nawata, "Performance Evaluation of Photovoltaic Power-Generation System Equipped With a Cooling Device Utilizing Siphonage," J. Sol. Energy Eng., Volume 128, Issue 2, pages 146-151, May 2006.

11 Riffat, S. B., Ma, X., "Thermoelectrics: a review of present and potential applications," Applied Thermal Engineering, Vol. 23, 2003, pp. 913–935.

12 Naito, H., Kohsaka, Y., Cooke, D., and Arashi, H., "Development of a solar receiver for a high-efficiency thermionic/thermoelectric conversion system," Solar Energy, Vol. 58, 1996, pp. 191–195.

13 Min, G., Rowe, D. M., and Kontostavlakis, K., "Thermoelectric figure-of-merit under large temperature differences," Journal of Physics D: Applied Physics, Vol. 37, 2004, pp. 1301–1304.

14 Quaschning, V., Understanding Renewable Energy Systems, Earthscan Publications, Ltd., 2005, Page 138.

15 Tester, J. W., Drake, E. M., Driscoll, M. J., Golay, M. W., Peters, W. A., Sustainable Energy Choosing Among Options, Massachusetts Institute of Technology Press, Cambridge, MA, 2005, p. 576.

16 Mills, A. F., Heat Transfer, 2nd Edition, Prentice Hall, Inc., 1999, Page 313.